

Continuous Force and Displacement Measurement Below the Standard Quantum Limit

David Mason^{1,2,*}, Junxin Chen^{1,2,*}, Massimiliano Rossi^{1,2,*}, Yeghishe Tsaturyan¹ & Albert Schliesser^{1,2,†}

¹*Niels Bohr Institute, University of Copenhagen, 2100 Copenhagen, Denmark*

²*Center for Hybrid Quantum Networks (Hy-Q), Niels Bohr Institute, University of Copenhagen, 2100 Copenhagen, Denmark*

*these authors contributed equally to this work

†to whom correspondence should be addressed; e-mail: albert.schliesser@nbi.ku.dk

Quantum mechanics dictates that the precision of physical measurements must be subject to certain constraints. In the case of interferometric displacement measurements, these restrictions impose a ‘standard quantum limit’ (SQL), which optimally balances the precision of a measurement with its unwanted backaction¹. To go beyond this limit, one must devise more sophisticated measurement techniques, which either ‘evade’ the backaction of the measurement², or achieve clever cancellation of the unwanted noise at the detector^{3,4}. In the half-century since the SQL was established, systems ranging from LIGO⁵ to ultracold atoms⁶ and nanomechanical devices^{7,8} have pushed displacement measurements towards this limit, and a variety of sub-SQL techniques have been tested in proof-of-principle experiments^{9–13}. However, to-date, no experimental system has successfully demonstrated an interferometric displacement measurement with sensitivity (including *all* relevant noise sources: thermal, backaction, and imprecision) below the SQL. Here, we exploit strong quantum correlations in an ultracoherent optomechanical system to demonstrate off-resonant force and displacement sensitivity reaching 1.5dB below the SQL. This achieves an outstanding goal in mechanical quantum sensing, and further enhances the prospects of using such devices for state-of-the-art force sensing applications.

The SQL can be derived through a straightforward analysis of the quantum noise sources in an ideal interferometric displacement measurement^{1,14–16}. The premise of such a measurement is that one couples the position of an object (say, a harmonically bound mirror) to the phase of a coherent light field. The uncertainty in this phase will scale inversely with the strength of the coherent field (as per the Heisenberg uncertainty relation). This imprecision noise (‘shot noise’) constitutes an effective displacement noise \hat{x}_{imp} , whose spectral density can be written as^{15,17}

$$\bar{S}_{xx}^{\text{imp}} = \frac{x_{\text{zpf}}^2}{4\Gamma_{\text{meas}}}, \quad (1)$$

where Γ_{meas} is a measurement rate¹⁷ characterizing the strength of the interaction, and $x_{\text{zpf}} = \sqrt{\hbar/2m\Omega_m}$ is the root-mean-square amplitude of the oscillator’s zero-point fluctuations (where m is the mass, Ω_m the resonance frequency, and \hbar the reduced Planck’s constant).

In addition to this imprecision noise, there will also be ‘backaction’ to the measurement, in the form of radiation pressure fluctuations (\hat{F}_{qba}). These fluctuations will be proportional to the measurement strength, with a spectral density given by

$$\bar{S}_{FF}^{\text{qba}} = \hbar^2 x_{\text{zpf}}^{-2} \Gamma_{\text{meas}}. \quad (2)$$

Through the mechanical susceptibility $\chi_m(\Omega) = m^{-1}(\Omega_m^2 - \Omega^2 - i\Gamma_m\Omega)^{-1}$ (where Γ_m is the mechanical energy damping rate), this produces displacement fluctuations, such that the total displacement noise added by the measurement process is given by:

$$\bar{S}_{xx}^{\text{add}}(\Omega) = \bar{S}_{xx}^{\text{imp}} + |\chi_m(\Omega)|^2 \bar{S}_{FF}^{\text{qba}}(\Omega). \quad (3)$$

Recalling how these terms scale with measurement strength, we see the fundamental tradeoff between imprecision and backaction in a displacement measurement. Minimizing with respect to the measurement strength, one finds that the minimum added noise occurs for $\Gamma_{\text{meas}}^{\text{opt}}(\Omega) = x_{\text{zpf}}^2 (2\hbar|\chi_m(\Omega)|)^{-1}$, at which point the two contributions are equal, and the minimum added noise, known as the SQL, is given by

$$\bar{S}_{xx}^{\text{SQL}}(\Omega) \equiv \min \bar{S}_{xx}^{\text{add}}(\Omega) = \hbar|\chi_m(\Omega)| \quad (4)$$

The added imprecision and backaction noise will appear in addition to the oscillator’s intrinsic motion, $\bar{S}_{xx}^{\text{int}}$, (consisting of zero-point motion and thermal motion), such that the *total* measured displacement noise is given by:

$$\bar{S}_{xx}^{\text{meas}}(\Omega) = \bar{S}_{xx}^{\text{int}}(\Omega) + \bar{S}_{xx}^{\text{add}}(\Omega) \quad (5)$$

These various contributions to the measured spectrum are illustrated in Fig. 1. Note that non-negligible thermal motion prevents measurements at the SQL on the mechanical resonance. As such, much of the progress in approaching the SQL in optomechanical systems has relied on first reducing the thermal motion, via cryogenics and laser cooling^{7,9}. Alternatively, if one

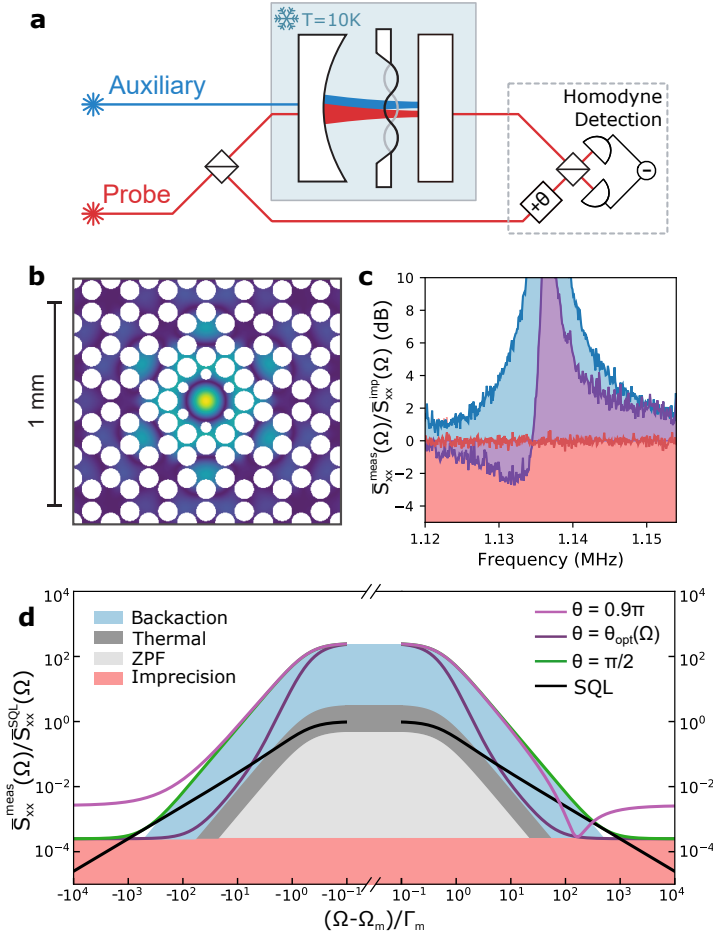


Figure 1: **Measuring beyond the standard quantum limit.** **a** Sketch of the experimental setup. **b** Simulated displacement pattern of the mechanical mode of interest. **c** Displacement spectra, normalized to the shot noise ($\bar{S}_{xx}^{\text{meas}}(\Omega)/\bar{S}_{xx}^{\text{imp}}(\Omega)$), demonstrating ponderomotive squeezing. Blue corresponds to a standard phase measurement ($\theta = \pi/2$), red indicates a shot noise measurement, and purple indicates a measurement of a rotated quadrature ($\theta \approx 0.16\pi$), for which strong correlations are visible. **d** Cartoon schematic of an interferometric displacement measurement. Shaded regions indicate different noise contributions, while the solid curves indicate the total spectra, under different measurement conditions: “standard” phase measurement (green), fixed “non-standard” quadrature measurement (light purple), frequency-dependent (“variational”) quadrature measurement (dark purple). The black line indicates the SQL.

can achieve quantum backaction noise which dominates over the thermal noise (as in Fig. 1), then there exist frequencies away from resonance where it is still possible reach the SQL. Indeed, the closest absolute approach to the SQL has recently been demonstrated in precisely this fashion⁸. Such broadband, off-resonance displacement measurements are relevant for many practical sensing applications, including gravitational wave detection.

While the SQL, as formulated above, does present a lower bound on the sensitivity of con-

ventional interferometry, it does not correspond to a fundamental quantum limit. Indeed, there are various ways to modify the premises of the measurement posed above, to enable sensitivities below the SQL^{18,19}. One well-known class of measurements avoids the required addition of backaction by measuring an observable which commutes with the system’s Hamiltonian, making a ‘quantum nondemolition’ (QND) or ‘backaction evading’ (BAE) measurement². Devices which couple either to the speed of a free mass^{20,21} (instead of displacement), or to a single mechanical quadrature^{22,23} satisfy this criteria, and indeed the latter has been demonstrated in several optomechanical systems^{10–12}, though with excess imprecision noise which prevented measurement below the SQL. Backaction-evading measurements of composite quadratures in multimode systems have also been explored in optomechanical²⁴ and hybrid spin-mechanical²⁵ systems. Still other techniques rely on modification of the mechanical susceptibility²⁶ (e.g. by creating an ‘optical spring’) to surpass the bare-resonator SQL (albeit establishing a new SQL at the shifted frequency).

Yet another class of measurements relies instead on the exploitation of quantum correlations to deviate from the SQL. Here, the underlying idea is that the derivation of the SQL assumed that the backaction and imprecision noises were uncorrelated (i.e. $\bar{S}_{xF}(\Omega) = 0$). Without this assumption, equation (3) reads (See Methods):

$$\bar{S}_{xx}^{\text{add}}(\Omega) = \bar{S}_{xx}^{\text{imp}} + |\chi_m(\Omega)|^2 \bar{S}_{FF}^{\text{qba}}(\Omega) + 2\text{Re} [\chi_m(\Omega)^* \bar{S}_{xF}(\Omega)]. \quad (6)$$

By utilizing correlations in the measurement spectrum, it is possible to arrange for destructive interference of the quantum imprecision and backaction noise. This can be achieved either by modifying the correlations of the input light (e.g. probing with squeezed instead of coherent light^{3,27–29}), or by taking advantage of optomechanically-induced correlations in the output light⁴. These correlations exist whenever backaction-dominated motion (arising from amplitude fluctuations of the optical field) is imprinted as phase fluctuations of that same field. These correlated fluctuations are the same which enable ponderomotive squeezing³⁰. To see these correlations, one simply needs to measure some mixed quadrature (containing both amplitude and phase fluctuations) of the optical field, as opposed to just making a phase measurement. Of course, measuring quadratures other than the optical phase will sacrifice some of the mechanical signal (i.e. increase the imprecision), but for some optical quadratures, the reduction in noise outweighs the loss in signal in a certain frequency band. This is illustrated in Fig. 1. Compared to the normal phase measurement (corresponding to a quadrature angle $\theta = \pi/2$), a detection angle of $\theta = 0.9\pi$ results in destructive interference of the backaction and imprecision near some particular frequency. A complete implementation of this ‘variational’ measurement actually envisions filtering the signal in such a way as to measure a frequency-dependent optical quadrature ($\theta_{\text{opt}}(\Omega)$), such that this interference occurs over a broad frequency range above and below resonance. This displacement sensitivity translates directly (via the susceptibility χ_m) into force sensitivity, as we will see later.

We note that exploiting quantum correlations in this way requires efficient optical detection, in addition to strong backaction. Any optical losses spoil the needed interference by substituting uncorrelated vacuum noise. Indeed, a recent work by Kampel et al.⁹ has provided an extensive

theoretical and experimental study of variational displacement measurements, but excess imprecision noise limited the sensitivity of the measurement to 0.9 dB above the SQL.

In this sense, while the principles underlying both BAE and variational techniques have been demonstrated, experiments to-date have fallen short of proving the original intent of these techniques, and interferometric force and displacement measurements beyond the SQL has remained an open experimental challenge³¹.

Here, we are able to address this challenge via an optomechanical system which permits strong, efficient quantum measurements, thanks to ultracoherent mechanical devices and carefully optimized optical readout. The mechanical system is based on a $3.6\text{mm} \times 3.6\text{mm} \times 20\text{nm}$ Si_3N_4 membrane, patterned with a honeycomb lattice of holes to create a phononic crystal (PnC) with an acoustic bandgap near 1 MHz. At the center of the membrane, a defect supports several localized, out-of-plane vibrational modes, whose frequencies lie within the bandgap. The PnC shields these modes from radiative loss, while simultaneously providing a “soft clamp”, which dramatically reduces the mechanical loss³². In this work, we focus on a single mode with resonance frequency $\Omega_m/2\pi = 1.135$ MHz and quality factor $Q = \Omega_m/\Gamma_m = 1.03 \times 10^9$ at temperature $T = 10$ K. The motion of the membrane is dispersively coupled to the resonance frequency of a Fabry-Pérot cavity mode (linewidth $\kappa/2\pi = 16.2$ MHz) at a characteristic vacuum coupling rate $g_0/2\pi = 120.7$ Hz. By driving the cavity mode near resonance, we populate a coherent field with average occupation \bar{n}_{cav} , which leads to a field-enhanced, linearized coupling at rate $g = g_0\sqrt{\bar{n}_{\text{cav}}}$. The cavity is highly over-coupled in transmission, such that 95% of the intracavity photons emerge towards the detector. We monitor the optical quadrature fluctuations of this output beam via a balanced homodyne detector, which can measure at an arbitrary quadrature angle, θ . By optimizing the output optics and homodyne detection, we achieve a total detection efficiency of $\eta_{\text{det}} = 77\%$. In addition to a resonant probe beam, we also use an auxiliary laser, addressing a separate cavity mode. This beam is used simultaneously for sideband cooling and as an actuator beam for feedback cooling of low-frequency out-of-bandgap membrane modes (for stabilization purposes⁸). This auxiliary beam also exerts a small amount of quantum backaction on the membrane, which we account for as an effective thermal bath (since it represents a source of uncorrelated force noise from the perspective of the probe beam). In the results which follow, it will be important that we know the transduction factor between mechanical displacement and photocurrent, for calibrating spectra. This is accomplished by a well-established phase modulation technique³³. This technique relies on knowledge of the optomechanical coupling rate, g_0 , which we obtain through two independent, cross-checked calibration methods (see Methods). We note that through these methods, we arrive at a calibration factor which enables robust comparison to the SQL, depending only on a few well-known system parameters (see Methods).

As noted previously, to exploit broadband correlations in the probe field, it is necessary that quantum backaction is the dominant source of force noise driving the resonator (as opposed to the thermal bath with mean phonon occupation \bar{n}_{th}). Quantitatively, this corresponds to reaching a “quantum cooperativity” $C_q = \Gamma_{\text{qba}}/\gamma \gtrsim 1$, where γ is the thermal decoherence rate of the oscillator and $\Gamma_{\text{qba}} = 4g^2/\kappa$ is the quantum backaction decoherence rate. Moreover, it is

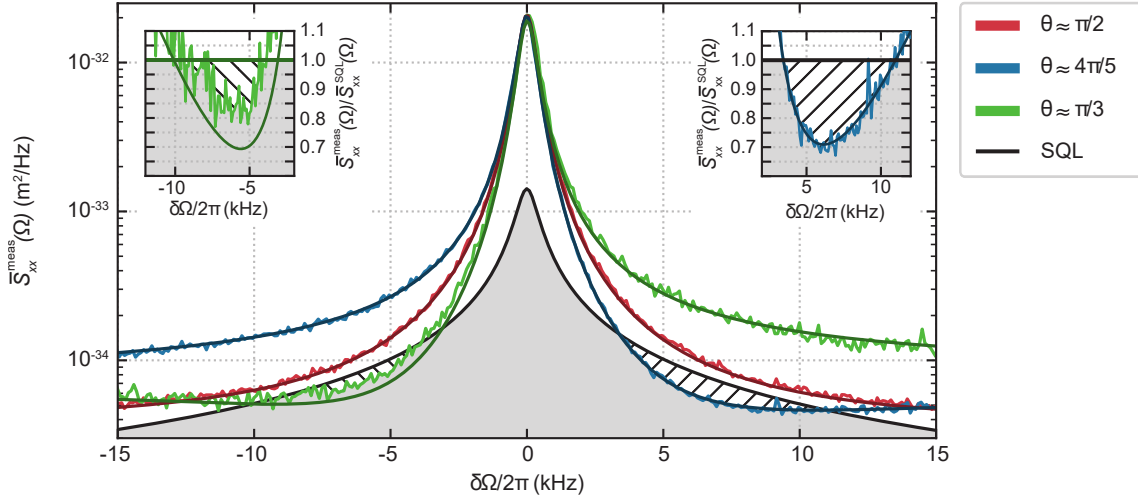


Figure 2: **Measuring displacement below the SQL.** Calibrated displacement spectra as measured at different quadrature angles of the homodyne receiver. The red curve corresponds to a ‘conventional’ ($\theta \approx \pi/2$) measurement, while blue and green correspond to quadratures which offer enhanced sensitivity above and below resonance, respectively. Solid dark color lines are fits to a complete model (see Method). The solid black line is the SQL of the effective oscillator. In the insets, a zoom of the hatched regions below and above resonance, where the noise level decreases below the SQL. Abscissa refers to frequency relative to the effective mechanical resonance $\delta\Omega = \Omega - \Omega_{\text{eff}}$.

important that the total detection efficiency is close to unity. A simple ponderomotive squeezing experiment (Fig. 1c) demonstrates that both of these are indeed satisfied in this system. We probe the motion with $C_q = 17.3$, and detect a homodyne quadrature corresponding to $\theta = 0.16 \pi$. The strong correlations produce the observed asymmetric Fano resonance.

Now, we examine what effect these correlations have on our displacement sensitivity, and compare with the SQL. Here, the SQL is defined as $\bar{S}_{xx}^{\text{SQL}}(\Omega) = \hbar |\chi_{\text{eff}}(\Omega)|$, where $\chi_{\text{eff}}(\Omega)$ is the effective mechanical susceptibility resulting from dynamical backaction of the (slightly red-detuned) probe and auxiliary lasers³⁴ (See Methods). Figure 2 shows three displacement spectra (for $C_q = 17.3$), one measured in a ‘‘standard’’ ($\theta \approx \pi/2$) configuration, and two measured at homodyne angles which are optimized for displacement sensitivity above and below resonance. We see that the correlations enable sub-SQL sensitivity in both regions, with the best sensitivity occurring at $\Omega - \Omega_{\text{m}}^{\text{eff}} = 2\pi \times 5.9$ kHz. Here, the total noise, including even thermal and zero-point fluctuations, is 1.5 dB below the SQL. The solid lines indicate predictions of standard optomechanical input-output theory¹⁵, in which three parameters (g , θ , and cavity detuning Δ) are adjusted to fit the data (see Methods). This is to account for small experimental drifts in intracavity power and laser detuning while we systematically vary the detection angle, θ .

Recalling Fig. 1, we note that different measurement angles optimize the sensitivity at different frequencies, and that larger backaction results in a larger frequency region in which correlations can be exploited. We demonstrate these dependencies in Fig. 3, which shows spectra

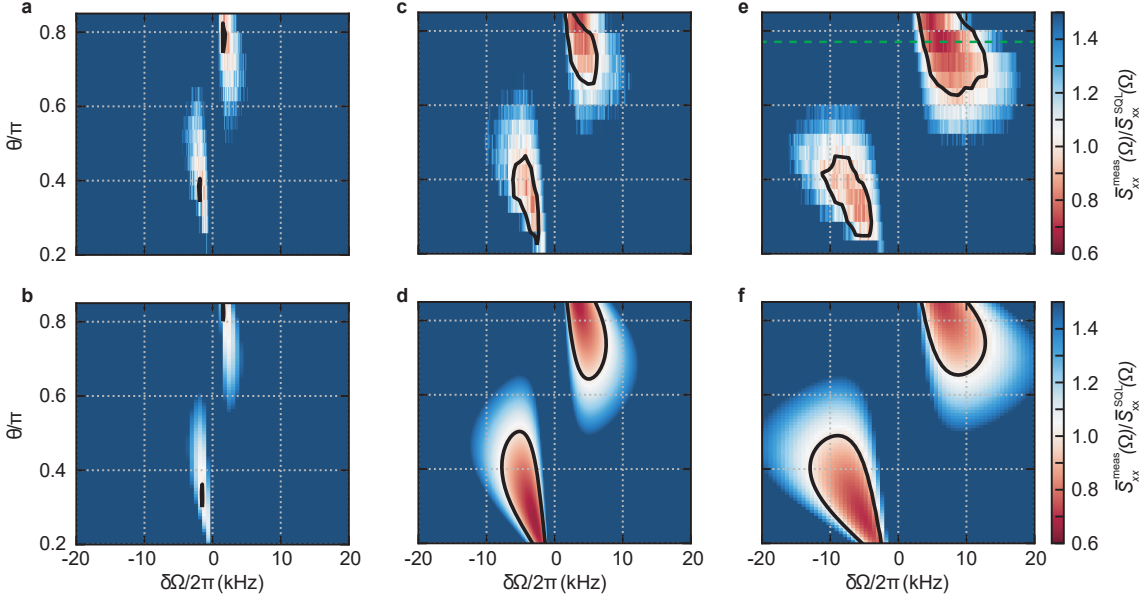


Figure 3: **Opening broadband regions of sub-SQL sensitivity.** **a, c, e** Calibrated displacement spectra (for $C_q = \{4.6, 8.8, 17.3\}$, respectively) near the mechanical resonance frequency Ω_{eff} , for varying measurement quadrature (θ). The spectra are divided by the SQL, such that red regions indicate sub-SQL sensitivity. Black contour lines corresponds to $\bar{S}_{xx}^{\text{meas}} = \bar{S}_{xx}^{\text{SQL}}$. The dashed green line in **e** corresponds to the blue spectrum in Fig. 2. **b, d, f** Independent predictions from the theoretical model (see Methods).

(normalized to the SQL) measured at various angles ($\theta \in [0.1\pi, 0.9\pi]$) and for $C_q = \{4.6, 8.8, 17.3\}$. We see that the bandwidth of sub-SQL performance is improved at larger values of C_q . Figure 3 shows theoretical spectra based purely on independent parameters, and we note broad consistency between the data and model throughout the parameter space. We note that the measurements generally show degraded performance on the lower-frequency side of resonance, which we attribute to the presence of extraneous cavity noise.

Sensitive displacement measurements are the foundation of sensitive force measurements. Here, we demonstrate proof-of-principle force measurements to illustrate how the signal-to-noise (SNR) ratio in such a measurement is improved through variational techniques, beyond what is possible at the SQL. We particularly emphasize how the signal and noise respond differently to measurement quadrature changes. By modulating the amplitude of the auxiliary laser, we apply a coherent, classical radiation pressure force on the mechanical resonator. We measure the response via homodyne detection as before, and compare with noise measurements as above. Figure 4 shows signal and noise measurements, in both raw voltage units and after using the calibration tone (and χ_{eff}) to calculate force spectra. The driven response at all frequencies is shown, with the signal at one frequency (Ω_0) emphasized for comparison. From the raw spectra (Fig. 4a), we note that between $\theta \approx \pi/2$ and $\theta \approx 4\pi/5$, the signal at $\Omega_0 - \Omega_{\text{eff}} = 2\pi \times 8.2$ kHz decreases by 1.9 dB (due to reduced motional transduction), while the noise level drops by 5.2 dB.

The reduced transduction is accounted for with our calibration method, such that in Fig. 4b we find equal force signals from both configurations (and for all frequencies), but still with reduced noise levels. The signal-to-noise ratio (SNR) is summarized in Fig. 4c, normalized to the SNR possible for a measurement operating at the SQL. (Note that we include in this noise floor the zero-point-fluctuations (ZPF), as they represent another fundamental noise source. In practice, this ZPF term³⁵ has a negligible impact in the frequency region where we find sub-SQL sensitivity). As in the noise-only measurements above, we find that the variational measurement enables SNR values exceeding what the SQL would allow over a 8 kHz bandwidth. Finally, we note that with the application of sub-SQL techniques, our force sensitivity, at Ω_0 , reaches $(11.2 \text{ aN}/\sqrt{\text{Hz}})^2$ – a number which can be improved significantly in low-mass versions of this system, optimized for force sensing.

The results presented here demonstrate that the position, even of a macroscopic object, can now be probed with a sensitivity reaching the limit which quantum mechanics imposes on conventional measurement. Moreover, we see how one can go beyond these limits by better using the quantum resources of the measurement (in this case, strong correlations). Indeed, in the sense that ponderomotive squeezing reflects entanglement between probe light sidebands³⁶, the technique demonstrated here can be considered a form of entanglement-enhanced measurement. The strong quantum interactions possible in this system should also allow explorations of similar quantum-enhanced measurement techniques, including synodyne detection³⁷ and single-quadrature measurements³⁸. It has also been shown that the limits of measurement-based quantum feedback (as was recently demonstrated in this system⁸) can be improved by exploiting variational techniques like the one shown here³⁹. Finally, the enhanced force sensitivity could be directly applicable in state-of-the-art force sensing applications⁴⁰, opening new regimes of precision measurement.

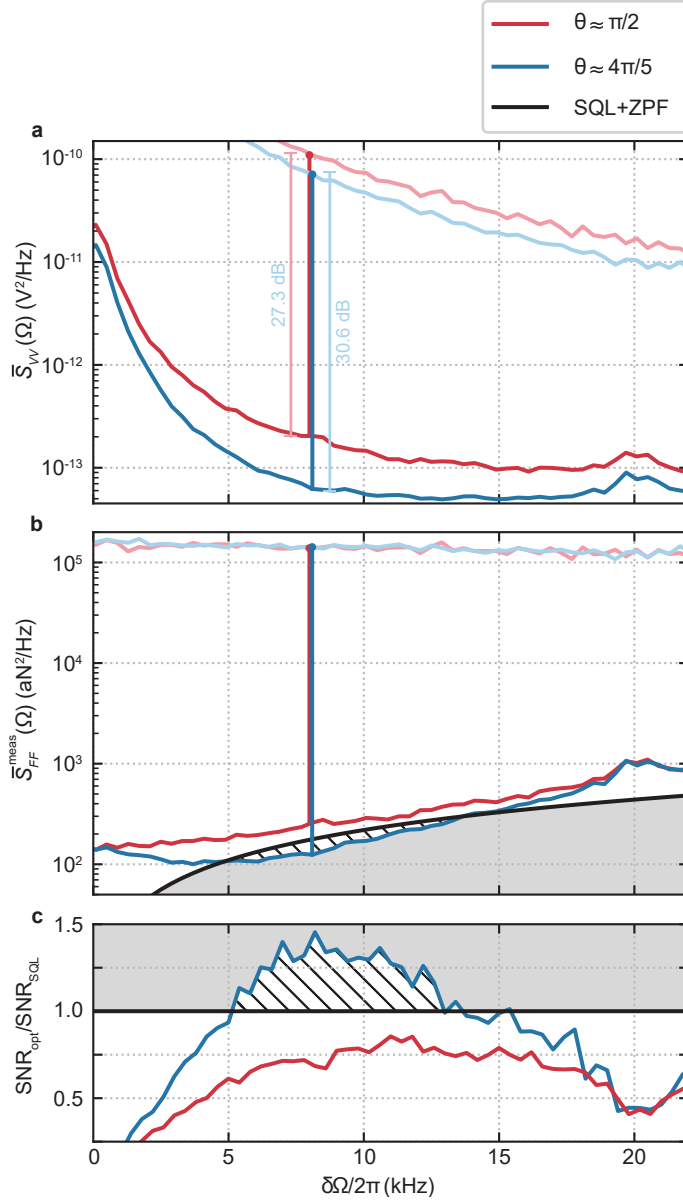


Figure 4: **Quantum-enhanced force sensing beyond the SQL.** **a**, Raw photocurrent spectra (dark lines) and driven response (light lines), for $\theta \approx \pi/2$ (red) and $\theta \approx 4\pi/5$ (blue). The response at $\delta\Omega/2\pi = 8.2\text{kHz}$ is highlighted for emphasis **b**, Same noise spectra and driven response measurements from **a**, calibrated in units of force noise. **c**, Signal-to-noise ratio (SNR), relative to the SNR of a measurement in which $\tilde{S}_{xx}^{\text{add}} = \tilde{S}_{xx}^{\text{SQL}}$.

Method

1 Model

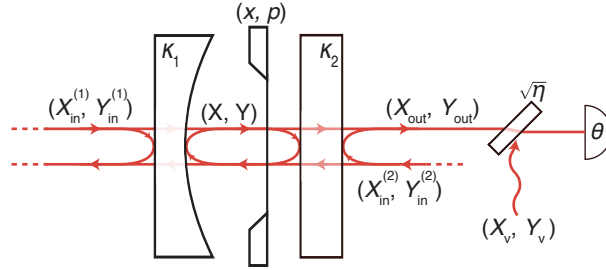


Figure 5: **Optomechanical cavity.** A coherent field drives a cavity mode from the left port. An homodyne receiver is set up to measure a quadrature θ of the transmitted field, through the right port of the cavity. Optical losses are modelled with uncorrelated vacuum entering from a beam-splitter with transmissivity η .

The homodyne spectra from the main text can be modelled within the standard framework of linearized optomechanics^{9,15,17}. In this way, the system dynamics are described by the following set of linear, coupled differential equations:

$$\dot{\hat{X}} = -\frac{\kappa}{2}\hat{X} - \Delta\hat{Y} + \sqrt{\kappa_1}\hat{X}_{\text{in}}^{(1)} + \sqrt{\kappa_2}\hat{X}_{\text{in}}^{(2)}, \quad (7a)$$

$$\dot{\hat{Y}} = -\frac{\kappa}{2}\hat{Y} + \Delta\hat{X} + 2g\frac{1}{\sqrt{2}x_{\text{zpf}}}\hat{x} + \sqrt{\kappa_1}\hat{Y}_{\text{in}}^{(1)} + \sqrt{\kappa_2}\hat{Y}_{\text{in}}^{(2)}, \quad (7b)$$

$$m\ddot{\hat{x}} = -m\Omega_{\text{m}}^2\hat{x} - m\Gamma_{\text{m}}\dot{\hat{x}} + 2g\frac{\hbar}{\sqrt{2}x_{\text{zpf}}}\hat{X} + \sqrt{\Gamma_{\text{m}}}\hat{F}_{\text{th}}, \quad (7c)$$

where \hat{X} , \hat{Y} and \hat{x} describe, respectively, the cavity amplitude and phase fluctuations and the mechanical position (Fig. 5). The loss rates through the two mirrors are given by κ_1 and κ_2 , and the total cavity decay rate is $\kappa = \kappa_1 + \kappa_2$. The thermal Langevin force (\hat{F}_{th}) satisfies $\langle \hat{F}_{\text{th}}(t)\hat{F}_{\text{th}}(t') \rangle = 2m\hbar\Omega_{\text{m}}(\bar{n}_{\text{th}} + 1/2)\delta(t - t')$. The terms $\hat{X}_{\text{in}}^{(i)}$ and $\hat{Y}_{\text{in}}^{(i)}$ represent, respectively, vacuum amplitude and phase fluctuations entering the i -th port of the cavity. Their correlations are

$$\langle \hat{X}_{\text{in}}^{(i)}(t)\hat{X}_{\text{in}}^{(j)}(t') \rangle = \langle \hat{Y}_{\text{in}}^{(i)}(t)\hat{Y}_{\text{in}}^{(j)}(t') \rangle = \frac{1}{2}\delta_{ij}\delta(t - t'), \quad (8a)$$

$$\langle \hat{X}_{\text{in}}^{(i)}(t)\hat{Y}_{\text{in}}^{(j)}(t') \rangle = \frac{i}{2}\delta_{ij}\delta(t - t'). \quad (8b)$$

This system has been considered in many excellent resources^{9,17}; for our starting point, we will consider a general quadrature of the transmitted output optical field,

$$\hat{X}_{\text{out}}^{\theta}(\Omega) = \hat{X}_{\text{in}}^{\theta} + f^{\theta}(\Omega)\hat{x}(\Omega), \quad (9)$$

where the mechanical position \hat{x} is transduced into quadrature fluctuations via the quadrature-dependent function $f^\theta(\Omega)$; $\hat{X}_{\text{in}}^\theta$ is a combination of input vacuum quadratures whose spectrum¹ is $S_{XX}^{\theta,\text{in}} = 1/2$. We note here that the angle θ is referred to the intracavity field, assumed real as phase reference. The transduction function is given by,

$$f^\theta(\Omega) = -i \frac{g}{\sqrt{2}x_{\text{zpf}}} \sqrt{\kappa_2} [\chi_c(\Omega)e^{i\theta} - \chi_c(-\Omega)^*e^{-i\theta}], \quad (10)$$

where $\chi_c(\Omega) = [\kappa/2 - i(\Delta + \Omega)]^{-1}$ is the cavity susceptibility. The position of the mechanical oscillator \hat{x} is

$$\hat{x}(\Omega) = \chi_{\text{eff}}(\Omega) [\hat{F}_{\text{th}}(\Omega) + \hat{F}_{\text{qba}}(\Omega)] \quad (11)$$

and it is driven by two forces: a Langevin force (\hat{F}_{th}) from the thermal bath and a quantum backaction force (\hat{F}_{qba}) from radiation pressure shot noise. They induce motion via the susceptibility $\chi_{\text{eff}}(\Omega)^{-1} = \chi_m(\Omega)^{-1} - i2g^2m\Omega_m [\chi_c(\Omega) - \chi_c(-\Omega)^*]$, effectively modified by dynamical backaction^{15,17}.

The output quadrature in equation (9) is measured by a balanced homodyne receiver. If optical losses are present, the unitless photocurrent becomes $I = \sqrt{\eta_{\text{det}}}\hat{X}_{\text{out}}^\theta + \sqrt{1 - \eta_{\text{det}}}\hat{X}_{\text{v}}$, with \hat{X}_{v} uncorrelated vacuum noise and η_{det} detection efficiency. To express the photocurrent in units of position, we divide I by $\sqrt{\eta_{\text{det}}}f^\theta(\Omega)$. Thus, the measured displacement is $\hat{x}_{\text{meas}} = \hat{x}_{\text{imp}} + \hat{x}$, where $x_{\text{meas}} = I/\sqrt{\eta_{\text{det}}}f^\theta(\Omega)$ and $x_{\text{imp}} = (\sqrt{\eta_{\text{det}}}\hat{X}_{\text{in}}^\theta + \sqrt{1 - \eta_{\text{det}}}\hat{X}_{\text{v}})/\sqrt{\eta_{\text{det}}}f^\theta(\Omega)$. The symmetrized spectrum is

$$\bar{S}_{xx}^{\text{meas}}(\Omega) = \bar{S}_{xx}^{\text{imp}}(\Omega) + |\chi_{\text{eff}}(\Omega)|^2 [\bar{S}_{FF}^{\text{th}}(\Omega) + \bar{S}_{FF}^{\text{qba}}(\Omega)] + 2\text{Re} [\chi_{\text{eff}}(\Omega)^* \bar{S}_{xF}(\Omega)]. \quad (12)$$

Different contributions can be identified. The input optical quadrature produces an apparent background (imprecision noise) given by

$$\bar{S}_{xx}^{\text{imp}}(\Omega) = \frac{x_{\text{zpf}}^2}{g^2\eta_{\text{det}}\kappa} \frac{1}{|\chi_c(\Omega)|^2 + |\chi_c(-\Omega)|^2 - 2\text{Re}[e^{i2\theta}\chi_c(\Omega)\chi_c(-\Omega)]}. \quad (13)$$

The quantum backaction force spectrum is given by

$$\bar{S}_{FF}^{\text{qba}}(\Omega) = \frac{\hbar^2}{2x_{\text{zpf}}^2} g^2\kappa (|\chi_c(\Omega)|^2 + |\chi_c(-\Omega)|^2), \quad (14)$$

while the thermal Langevin force is $\bar{S}_{FF}^{\text{th}}(\Omega) = m\Gamma_m\hbar\Omega_m(2\bar{n}_{\text{th}} + 1)$. Finally, the last term appears because, generally speaking, the quantum backaction force and the imprecision noise are caused by partially the same fluctuations. Properly taking these correlations into account gives

$$\bar{S}_{xF}(\Omega) = \frac{\hbar}{2i} \frac{\chi_c(\Omega)e^{i\theta} + \chi_c(-\Omega)^*e^{-i\theta}}{\chi_c(\Omega)e^{i\theta} - \chi_c(-\Omega)^*e^{-i\theta}}. \quad (15)$$

¹We use a double-sided spectral convention, where $S_{AB}(\Omega) = \int_{-\infty}^{\infty} dt e^{i\Omega t} \langle \hat{A}^\dagger(t)\hat{B}(0) \rangle$. Symmetrisation, i.e. $\bar{S}_{AB}(\Omega) = (S_{AB}(\Omega) + S_{AB}(-\Omega))/2$ is indicated by a overbar.

Note that by setting this correlation term to zero in equation 12, and optimizing the combined imprecision and backaction, one can find the SQL as used in the main text: $\bar{S}_{xx}^{\text{SQL}}(\Omega) = \hbar|\chi_{\text{eff}}(\Omega)|$.

In the resonant case ($\Delta = 0$) and for a “bad cavity” ($\kappa \gg \Omega_m$) the previous contributions can be simplified. The imprecision noise becomes

$$\bar{S}_{xx}^{\text{imp}}(\Omega) \approx \frac{x_{\text{zpf}}^2}{16g^2\eta_{\text{det}}/\kappa} \frac{1}{\sin^2 \theta}, \quad (16)$$

which is minimized for a phase measurement, i.e. $\theta = \pi/2$. The quantum backaction force, independent from the measured quadrature, becomes

$$\bar{S}_{FF}^{\text{qba}}(\Omega) \approx \frac{\hbar^2}{2x_{\text{zpf}}^2} \frac{8g^2}{\kappa} \quad (17)$$

and the correlation term is

$$\bar{S}_{xF}(\Omega) \approx -\frac{\hbar}{2} \cot \theta. \quad (18)$$

2 Model fit

The model in equation (12) is used to fit measured photocurrent, calibrated in absolute displacement units (see below). To account for slow drifts of parameters during the experiment, we fit the homodyne angle θ , the coupling g , and the detuning Δ (Fig. 6a-d). The asymmetric line-shape due to correlations is reproduced by the fit model, as shown in Figure 6d. All the other parameters which enter in equation (12) are fixed by independent measurement and predictions.

In particular, the detection efficiency η_{det} is derived from fitting the calibrated shot noise level ($\bar{S}_{xx}^{\text{imp}}$) as a function of θ (equation (13)), as shown in Fig. 7.

We notice a strong correlation between the parameters \tilde{g} and $\tilde{\Delta}$ from the fit. This can be explained with variation of the input probe power. In fact, it directly changes the intracavity photon number \bar{n}_{cav} and, thus, g . At the same time, a power drift changes the setpoint at which the detuning Δ is stabilized through a Pound-Drever-Hall lock with a non-zero offset.

3 Calibration

When making absolute comparisons to the SQL, careful calibration of the noise spectra is of key importance. Here we detail our approach, which is fundamentally based on using quantum backaction as a calibrated thermal bath. Additional details about this method are also available in our previous work⁸.

The calibration is composed of two steps. First, we conduct a sideband cooling experiment, in order to establish a well-known temperature reference. This involves monitoring the

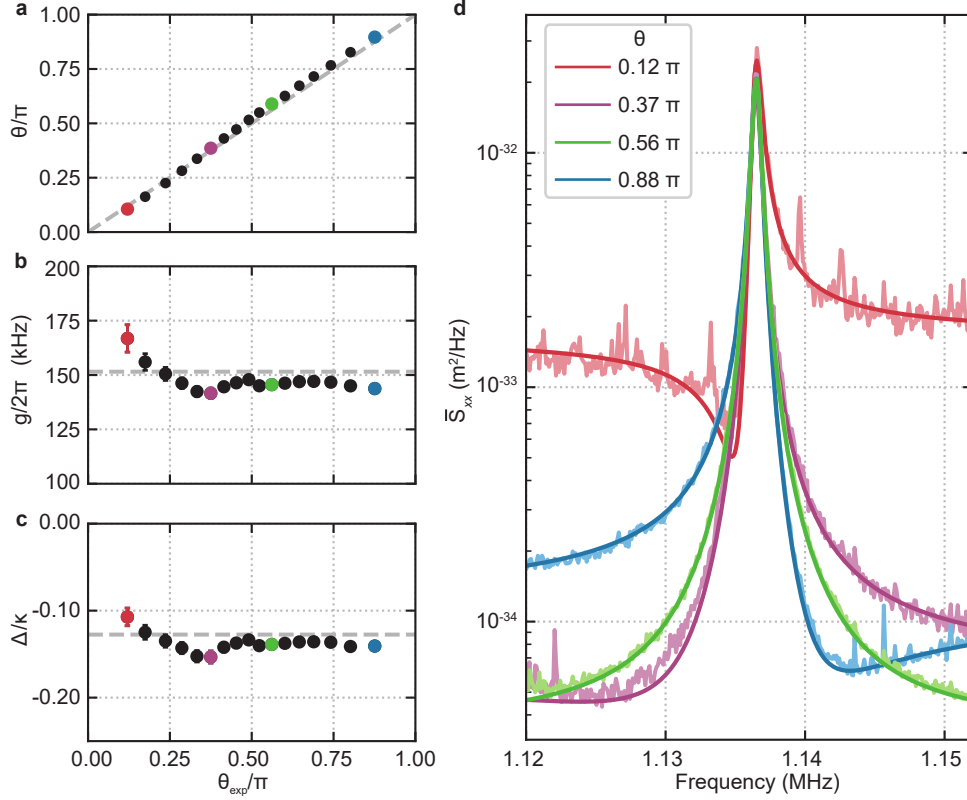


Figure 6: **Fit of displacement spectra.** **a–c**, Fitted parameters from the spectra of the measured photocurrent. Dashed gray lines are predictions from independent measurements. **d**, Example of measured spectra (light) and fit (dark). The corresponding fitted parameters are marked, with the same colours, in **a–c**.

motion with a weak probe beam, while an auxiliary beam (with detuning $\Delta_{\text{aux}} = -0.33\kappa_{\text{aux}}$, where κ_{aux} is the auxiliary cavity mode linewidth) is used to sideband cool the mechanical mode, reaching an asymptotic phonon occupancy (\bar{n}_{min}) set by quantum backaction (QBA). This backaction provides a well-known bath to define the temperature of the mechanics. This motion translates to cavity frequency noise via the optomechanical coupling, g_0 as follows:

$$\langle \delta\Omega^2 \rangle_{\text{mech}}^{\text{QBA}} = 2g_0^2 \left(\bar{n}_{\text{min}} + \frac{1}{2} \right), \quad (19)$$

The transduction factor of this frequency noise into voltage noise is measured via a calibrated phase modulation tone at frequency $\Omega_{\text{cal}} \approx \Omega_{\text{m}}$:

$$K = \frac{\langle \delta V^2 \rangle_{\text{cal}}^{\text{QBA}}}{\langle \delta\phi^2 \rangle_{\text{cal}}^{\text{QBA}}} = \frac{\langle \delta V^2 \rangle_{\text{cal}}^{\text{QBA}}}{\phi^2/2}, \quad (20)$$

where ϕ the phase modulation depth of the calibration tone. Thus, the measured voltage vari-

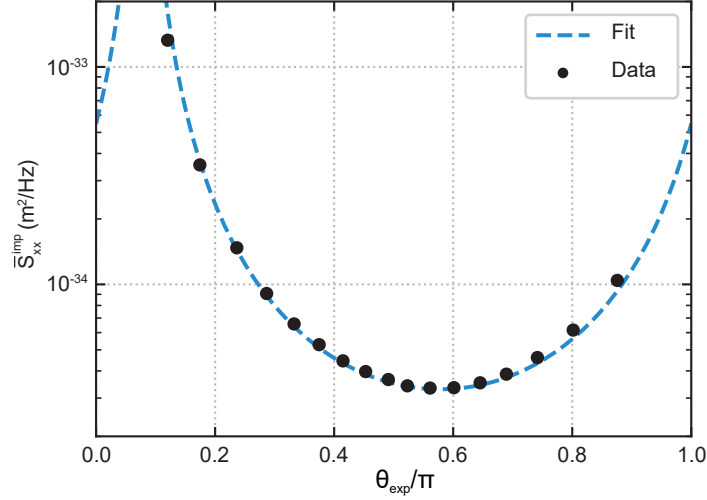


Figure 7: **Calibrated imprecision noise.** By means of phase modulation technique, the homodyne receiver shot noise level is calibrated into displacement imprecision noise, for different measured quadratures θ . From a fit the detection efficiency η is derived.

ance due to mechanical motion can be expressed in terms of frequency variance as

$$\langle \delta V^2 \rangle_{\text{mech}}^{\text{QBA}} = K \langle \delta \phi^2 \rangle_{\text{mech}}^{\text{QBA}} = K \langle \delta \Omega^2 \rangle_{\text{mech}}^{\text{QBA}} / \Omega_m^2 = \frac{K 2g_0^2}{\Omega_m^2} \left(\bar{n}_{\text{min}} + \frac{1}{2} \right). \quad (21)$$

Substituting K from equation (20), and solving for g_0 , we have

$$g_0 = \sqrt{\frac{\langle \delta V^2 \rangle_{\text{mech}}^{\text{QBA}} \Omega_m^2 \phi^2 / 2}{\langle \delta V^2 \rangle_{\text{cal}}^{\text{QBA}} 2(\bar{n}_{\text{min}} + 1/2)}}. \quad (22)$$

From this measurement, we find $g_0/2\pi = 120.7$ Hz. Actually we fit g_0 from the entire sideband cooling dataset (various cooling powers), to provide a more robust g_0 estimate, as well as an estimate of the thermal bath temperature. As a cross-check, we also conduct an optomechanically-induced transparency (OMIT) experiment, which also calibrates g_0 , but relying on a different set of parameter assumptions. The OMIT calibration only differs from the backaction calibration by 3% ($g_0/2\pi = 124.7$ Hz).

With g_0 obtained, we can now use the same calibration technique to convert arbitrary voltage spectra (\bar{S}_{VV}) into displacement spectra ($\bar{S}_{xx}^{\text{meas}}$)³³ [Gorodetsky2010]:

$$\bar{S}_{xx}^{\text{meas}} = \frac{x_{\text{zpf}}^2 \Omega_m^2 \phi^2 / 2}{g_0^2 \langle \delta V^2 \rangle_{\text{cal}}^{\text{meas}}} \bar{S}_{VV}, \quad (23)$$

where $\langle \delta V^2 \rangle_{\text{cal}}^{\text{meas}}$ is the voltage variance of the calibration tone in that particular measurement. Note that this is different from $\langle \delta V^2 \rangle_{\text{cal}}^{\text{QBA}}$, which refers specifically to the calibration tone voltage during the QBA calibration measurement.

Using equation (22) we recast this conversion factor as:

$$\bar{S}_{xx}^{\text{meas}} = \frac{x_{\text{zpf}}^2(2\bar{n}_{\text{min}} + 1)}{\langle \delta V^2 \rangle_{\text{mech}}^{\text{QBA}}} \frac{\langle \delta V^2 \rangle_{\text{cal}}^{\text{QBA}}}{\langle \delta V^2 \rangle_{\text{cal}}^{\text{meas}}} \bar{S}_{VV}. \quad (24)$$

We note that even the modulation depth of the calibration tone has now cancelled out. The only parameters which remain are several precisely-known frequencies, \bar{n}_{min} (which itself depends only on three well-known variables: κ_{aux} , Δ_{aux} , and Ω_{m}), x_{zpf} , and a few voltages which are read directly from various spectra. The only remaining uncertainty might be in x_{zpf} , due to its dependence on the oscillator mass, but since $\bar{S}_{xx}^{\text{SQL}} = \hbar|\chi_{\text{m}}| = \hbar m^{-1} / \sqrt{(\Omega_{\text{m}}^2 - \Omega^2)^2 + \Gamma_{\text{m}}^2 \Omega^2}$ has the same mass-dependence, our figure-of-merit comparisons remain robust:

$$\frac{\bar{S}_{xx}^{\text{meas}}}{\bar{S}_{xx}^{\text{SQL}}} = \frac{\Omega_{\text{m}}(\bar{n}_{\text{min}} + 1/2) \sqrt{(\Omega_{\text{m}}^2 - \Omega^2)^2 + \Gamma_{\text{m}}^2 \Omega^2}}{\langle \delta V^2 \rangle_{\text{mech}}^{\text{QBA}} \Omega_{\text{cal}}^2} \frac{\langle \delta V^2 \rangle_{\text{cal}}^{\text{QBA}}}{\langle \delta V^2 \rangle_{\text{cal}}^{\text{meas}}} \bar{S}_{VV}. \quad (25)$$

References

- [1] Braginsky, V. B. Classical and quantum restrictions on the detection of weak disturbances of a macroscopic oscillator. J. Exp. Theor. Phys **26**, 831–834 (1968).
- [2] Braginsky, V., Vorontsov, Y. & Thorne, K. Quantum Nondemolition Measurements. Science **209**, 547–557 (1980).
- [3] Unruh, W. Quantum Noise in the Interferometer Detector. In Meystre, P. & Scully, M. O. (eds.) Quantum Optics, Experimental Gravitation, and Measurement Theory, 647 (Plenum, New York, 1982).
- [4] Vyatchanin, S. P. & Zubova, E. A. Quantum variation measurement of a force. Phys. Lett. A **201**, 269–274 (1995).
- [5] Aasi, J. et al. Enhanced sensitivity of the LIGO gravitational wave detector by using squeezed states of light. Nat. Photonics **7** (2013).
- [6] Schreppler, S. et al. Optically measuring force near the standard quantum limit. Science **344**, 1486–1489 (2014).
- [7] LaHaye, M. D., Buu, O., Camarota, B. & Schwab, K. C. Approaching the quantum limit of a nanomechanical resonator. Science **304**, 74–7 (2004).
- [8] Rossi, M., Mason, D., Chen, J., Tsaturyan, Y. & Schliesser, A. Measurement-based quantum control of mechanical motion. Nature (accepted). [arXiv:1805.05087](https://arxiv.org/abs/1805.05087).
- [9] Kampel, N. S. et al. Improving broadband displacement detection with quantum correlations. Phys. Rev. X **7** (2017).
- [10] Suh, J. et al. Mechanically detecting and avoiding the quantum fluctuations of a microwave field. Science **344**, 1262–1265 (2014).
- [11] Wollman, E. E. et al. Quantum squeezing of motion in a mechanical resonator. Science **349**, 952–5 (2015).
- [12] Lecocq, F., Clark, J. B., Simmonds, R. W., Aumentado, J. & Teufel, J. D. Quantum Nondemolition Measurement of a Nonclassical State of a Massive Object. Phys. Rev. X **5**, 041037 (2015).
- [13] Sudhir, V. et al. Quantum correlations of light from a room-temperature mechanical oscillator. Physical Review X **7** (2017).
- [14] Clerk, A. A., Devoret, M. H., Girvin, S. M., Marquardt, F. & Schoelkopf, R. J. Introduction to quantum noise, measurement, and amplification. Rev. Mod. Phys **82**, 1155–1208 (2010).

- [15] Aspelmeyer, M., Kippenberg, T. J. & Marquardt, F. Cavity optomechanics. Rev. Mod. Phys **86**, 1391–1452 (2014).
- [16] Braginsky, V. B., Khalili, F. Y. & Thorne, K. S. Quantum Measurement (Cambridge University Press, Cambridge, 1992).
- [17] Bowen, W. P. & Milburn, G. J. Quantum Optomechanics (CRC Press, 2016).
- [18] Kimble, H. J., Levin, Y., Matsko, A. B., Thorne, K. S. & Vyatchanin, S. P. Conversion of conventional gravitational-wave interferometers into quantum nondemolition interferometers by modifying their input and/or output optics. Phys. Rev. D **65** (2002).
- [19] Corbitt, T. & Mavalvala, N. Quantum noise in gravitational-wave interferometers. In J. Opt. B: Quantum Semiclass. Opt., vol. 6 (2004).
- [20] Braginsky, V. & Khalili, F. Gravitational wave antenna with QND speed meter. Phys. Lett. A **147**, 251–256 (1990).
- [21] Purdue, P. & Chen, Y. Practical speed meter designs for quantum nondemolition gravitational-wave interferometers. Phys. Rev. D **66** (2002).
- [22] Thorne, K. S., Drever, R. W., Caves, C. M., Zimmermann, M. & Sandberg, V. D. Quantum nondemolition measurements of harmonic oscillators. Phys. Rev. Lett **40**, 667–671 (1978).
- [23] Braginskii, V. B., Vorontsov, Y. I. & Khalili, F. Y. Optimal quantum measurements in detectors of gravitation radiation. Soviet Journal of Experimental and Theoretical Physics Letters **27**, 276 (1978).
- [24] Ockeloen-Korppi, C. F. et al. Quantum Backaction Evading Measurement of Collective Mechanical Modes. Physical Review Letters **117** (2016).
- [25] Møller, C. B. et al. Quantum back-action-evading measurement of motion in a negative mass reference frame. Nature Publishing Group **547** (2017).
- [26] Arcizet, O., Briant, T., Heidmann, A. & Pinard, M. Beating quantum limits in an optomechanical sensor by cavity detuning. Physical Review A - Atomic, Molecular, and Optical Physics **73** (2006).
- [27] Caves, C. M. Quantum-mechanical noise in an interferometer. Phys. Rev. D **23**, 1693–1708 (1981).
- [28] Hoff, U. B. et al. Quantum-enhanced micromechanical displacement sensitivity. Optics Letters **38**, 1413 (2013).

- [29] LIGO Scientific Collaboration, T. A gravitational wave observatory operating beyond the quantum shot-noise limit (2011).
- [30] Braginsky, V. B. & Manukin, A. B. Ponderomotive effects of electromagnetic radiation. Soviet Physics JETP **25**, 653–655 (1967).
- [31] Giovannetti, V., Lloyd, S. & Maccone, L. Quantum Enhanced Measurement: Beating the Standard Quantum Limit. Science **306**, 1330–6 (2004).
- [32] Tsaturyan, Y., Barg, A., Polzik, E. S. & Schliesser, A. Ultracoherent nanomechanical resonators via soft clamping and dissipation dilution. Nat. Nanotechnol (2017).
- [33] Gorodetsky, M., Schliesser, A., Anetsberger, G., Deleglise, S. & Kippenberg, T. J. Determination of the vacuum optomechanical coupling rate using frequency noise calibration. Opt. Express **18**, 23236 (2010).
- [34] Clerk, A. A. Optomechanics and quantum measurement. Les Houches 2015 Summer School on Optomechanics.
- [35] Clerk, A. A. Quantum-limited position detection and amplification: A linear response perspective. Phys. Rev. B **70**, 1–9 (2004).
- [36] Zippilli, S., Di Giuseppe, G. & Vitali, D. Entanglement and squeezing of continuous-wave stationary light. New J. Phys **17** (2015).
- [37] Buchmann, L. F., Schreppler, S., Kohler, J., Spethmann, N. & Stamper-Kurn, D. M. Complex Squeezing and Force Measurement beyond the Standard Quantum Limit. Phys. Rev. Lett **117** (2016).
- [38] Clerk, A. A., Marquardt, F. & Jacobs, K. Back-action evasion and squeezing of a mechanical resonator using a cavity detector. New J. Phys **10** (2008).
- [39] Habibi, H., Zeuthen, E., Ghanaatshoar, M. & Hammerer, K. Quantum Feedback Cooling of a Mechanical Oscillator Using Variational Measurements: Tweaking Heisenberg’s Microscope. J. Opt. **18**, 084004 (2016).
- [40] Poggio, M. & Degen, C. L. Force-detected nuclear magnetic resonance: recent advances and future challenges. Nanotechnology **21**, 342001 (2010).